ACI STRUCTURAL JOURNAL TECHNICAL PAPER

Title No. 115-S38

Risk-Informed Condition Assessment of a Bridge with Alkali-Aggregate Reaction

by Mohammad Amin Hariri-Ardebili, Victor E. Saouma, and Christine Merz

This paper reports on a computational framework that assesses the integrity of a structure suffering from alkali-aggregate reaction (AAR). First, detailed field observation and laboratory tests are performed. Results were then interpreted in a format suitable for structural analysis. Then, probabilistic-based three-dimensional (3-D) nonlinear finite element simulations were performed. Preliminary results (deformation and stress field) were completely unintuitive and highlighted the complexity of the impact of AAR on a structural response. Results were cast in a risk-informed condition assessment framework through a new paradigm for AAR, based on work in the field of earthquake engineering. This procedure allows engineers to address two questions: 1) What is the anticipated level of damage at a given time? and 2) What is the time frame within which a given damage may occur? For this investigation, a major viaduct in Switzerland is analyzed.

Keywords: alkali-aggregate reaction (AAR); damage; fragility; residual expansion; uncertainty; viaduct.

INTRODUCTION

With the aging of infrastructure, alkali-aggregate reaction (AAR) becomes increasingly apparent as most of the structures were built at a time when the nature of the reaction was poorly understood, and standards for the detection of potential AAR in concrete mixtures were not well established. Whereas the problem has been traditionally associated with dams, it has also affected numerous bridges worldwide.[1] In an early study,[2] it was reported that in Denmark 600 bridges (roads and railways) and an unknown number of municipal ones are potentially AAR dangerous.

In a widely reported case, AAR expansion has caused rupture of the reinforcement.[3] The 6th Street Viaduct in Los Angeles was constructed in 1932 using what was then state-of-the-art concrete technology and the use of an on-site batching plant. Yet, over the past 75 years, concrete elements have cracked and deteriorated due to AAR. As a result, the viaduct's concrete has lost significant strength, and the structure is subject to failure under predictable seismic loads.[4] The bridge was recently dismantled and became yet another casualty of AAR.

Studies have mostly focused on field observations and assessments[5-7] where not only residual expansions are measured but increasingly petrographic analyses are also performed.[8-10] It has not been unusual to replace a structure on the sole basis of field/petrographic study without an attempt to conceptualize findings into engineering parameters that can be used by structural engineers for a final structural integrity assessment.

To the best of the authors' knowledge, there have been very few publications related to "science-based" numerical prediction of the structural response of bridges affected by AAR. Indeed, the FHWA Report[11] does not even mention the term "finite element" once in its 154 pages.

Most recently, the deterministic finite element simulation of a viaduct[12] undergoing a delayed ettringite formation (a swelling reaction so similar to AAR that the quasi-identical swelling model is adopted) was reported. Regretfully, very little details (if any) are provided regarding the numerical assumptions of the model, and how they are obtained. Huang et al.[13] presented an interesting probabilistic-based investigation of the steel-concrete bond in AAR-affected structures. The deterministic analysis of an entire bridge, albeit with a rather simplified model, was reported in Wojslaw andWisniewski.[14] It highlighted a potential deficiency in shear,[15] where a set of parametric analyses on shear capacity of concrete beams and panels are performed. A multi-linear regression model based on Akaike and Bayesian information criterion is used to quantify the most sensitive parameters.

This paper studies a major precast segmental bridge in Switzerland (commonly referred to as the *Viaduct de Chillon*) that was recently found to suffer from AAR (albeit at an early stage) and as a result underwent major rehabilitation.[16] First, the existing information on field and laboratory tests (petrographic, mechanical, and residual expansion tests) will be critically reviewed and findings reinterpreted in terms suitable for a finite element structural analysis (with wide margins of uncertainties). Then, given those uncertainties, an innovative probabilistic-based model, inspired by Latin Hypercube Sampling (LHS), is proposed. This model is then applied to run a large set of analyses. Finally, predictive results are presented and appropriate conclusions drawn.

RESEARCH SIGNIFICANCE

Altthough AAR has been a major concern in countless bridges, it has received little attention in terms of numerical simulation. This paper merges the expertise of material scientists and the one of structural engineers who have traditionally spoken different "dialects" and very seldom together.

Another novelty of this paper is the combination of fundamental theory, computation, probabilistic analysis, and field data to provide a more rational prediction for future behavior. Most importantly, this paper provides a novel framework for

ACI Structural Journal, V. 115, No. 2, March 2018.
MS No. S-2017-080.R2, doi: 10.14359/51701106, was received April 19, 2017, and reviewed under Institute publication policies.

Fig. 1—General view of viaduct.[18]

a rigorous risk-informed condition assessment for structures affected by AAR.

DESCRIPTION OF VIADUCT

The *Viaduct de Chillon* is a precast post-tensioned bridge spanning between 92 and 104 m (301.8 and 341.2 ft) over a total length of 2120 m (6955.4 ft). The French double-cantilever construction system was used with precast *voussoirs*. It was opened to traffic in 1969 and is a well-known innovative and iconic structure widely recognized[17] (Fig. 1).

CONCRETE CONDITIONS

Scheduled inspections have revealed a significant increase in reinforcement corrosion due to chloride diffusion through cracks. Ensuing preliminary investigations of the deck (concrete compressive strength, mild and prestressing steel tensile strength) were performed and repairs were conducted from 2012 to 2013. However, poor adhesion of the repair overlay mortar to the subjacent concrete was observed. Should the concrete have been sound, this should not have occurred, and as such, AAR was strongly suspected. In 2012, many samples were extracted along the nearly 2 km (6562 ft) length of the bridge to properly account for the inherent and inevitable variabilities encountered in such a structure. Cores were extracted from the slabs and webs and not from the inclined segments as their structural role was perceived as minimal. Tests included microscopic analysis (composition and microstructure, state of degradation), residual expansion measurements, compressive strength of cores, direct tensile strength, tensile axial splitting, static elastic modulus in compression, and hardened concrete mass density. Findings[18] led to the following observations.

Topological damage distribution—The central zone of the deck exhibited most deterioration. This may be related to concrete casting, storage, and curing conditions. Indeed, segregation and bleeding of the fresh concrete may have caused microstructural weaknesses. Traffic, temperature changes, and exposure to deicing salts also constituted aggravating factors.

Concrete degradation—The aggregates used come from a mixture of silica and silicate metamorphic rocks of sedimentary and crystalline nature, with a slow/late reaction potential. The portland cement content of the deck ranged from 350 to 400 kg/m^3 (21.9 to 25.0 lb/ft^3) (350 kg/m^3 [21.9 lb/ft^3] specified).

So far, concrete has undergone relatively small expansions, as it has been in a relatively dry condition (there were no visible signs of microcracks), and the potential for expansion is intact. It is estimated that present (45 years after construction) expansion is less than 0.1% and that future expansion (after an additional 45 years) should be between approximately 0.4 and 0.9% based on petrographic report.[18]

Expansion tests have not revealed a "plateau"; this is often the case when aggregates do also contain alkali. It was estimated that the laboratory maximum rate of expansion is 0.7 to 0.8 mm/m/y (8.4×10^{-3} to 9.6×10^{-3} in./ft/y). Based on Arrhenius law, it is estimated that at 11°C (52°F) expansion is approximately five times slower than at 38°C (100°F), yielding a guesstimate 0.1 to 0.2 mm/m/y (1.2×10^{-3} to 2.4×10^{3} in./ft/y) in the worst-case scenario. This in turn will result in 0.45 to 0.9% future expansion in the most unfavorable conditions—that is, wet surfaces without protection. Indeed, this concrete was labeled as one of the most reactive concretes known in Switzerland. However, it should be noted that true field expansion is most often a fraction of what has been measured in the laboratory. Correlation between the two is not trivial, as a slightly different reaction occurs at lower temperature and smaller RH than in the laboratory. This reduction was not accounted for in this study, which focused on "worst-case scenario" in the context of a probabilistic approach.[37]

Mechanical properties were obtained from 100 mm (3.94 in.) diameter cores and maximum aggregate size of 32 mm (1.26 in.). Values are shown in Table 1 and corresponding percentage losses (determined from concrete in unaffected zones) are also shown. The mechanical properties of the inclined members were not tested, as they play a relatively minor structural role. Besides, the concrete used in these components is likely to have been quite different than the one used in the main box girder. Finally, in anticipation of a possible strengthening, a crude estimate of the possible evolution of mechanical strength in the next 30 years has been attempted[18] (Table 1).

Remedial

The conclusions attributing the damage to AAR, it was decided to strengthen the whole bridge deck by adding a layer of 40 mm (1.57 in.) of an ultra-high-performance fiber-reinforced cement-based composite (UHPFRC) material, reinforced with steel reinforcing bars. Strain-hardening UHPFRC with its low permeability is an ideal sealant to reduce ingress of water and thus slow/stop AAR expansion.[16]

CONSTITUTIVE MODEL FOR AAR

The theoretical underpinning of the model used in this paper has been presented by one of the authors separately.[19,20] The AAR expansion is considered to be volumetric and formulated by the following kinetics law

$$\xi(t,\theta) = \frac{1-\exp\left(-\dfrac{t}{\tau_c(\theta)}\right)}{1+\exp\left(-\dfrac{\left(t-\tau_l(\theta)\right)}{\tau_c(\theta)}\right)} \quad (1)$$

Table 1—Mean and minimum values of concrete properties[18]

Current (year 2015, age 45 years)									
Property	Intact	Mean values degraded				Minimum values degraded			
	Bottom	Center top	Loss %	Bottom side	Loss %	Center top	Loss %	Bottom side	Loss %
f_c', MPa	90 ± 10	75 ± 10	5 to 20	90 ± 10	0	65	30	80	10
f_t', MPa	4.5 ± 0.5	2.5 ± 0.7	40 to 45	3.7 ± 0.7	15 to 20	1.8	60	3.0	30
E, GPa	40 ± 4	32 ± 4	15 to 20	38 ± 4	0 to 5	28	30	30	15
Projected (year 2045, age 75 years)									
f_c', MPa	90 ± 10	55 ± 10	35 to 40	70 ± 10	20 to 25	40	30	55	10
f_t', MPa	4.5 ± 0.5	2.0 ± 1.0	50 to 60	2.0 ± 1.0	30 to 35	1.0	60	2.0	30
E, GPa	40 ± 4	25 ± 5	30 to 35	30 ± 5	20 to 25	21	30	25	15

Notes: 1 MPa = 145 psi; 1 GPa = 145 ksi.

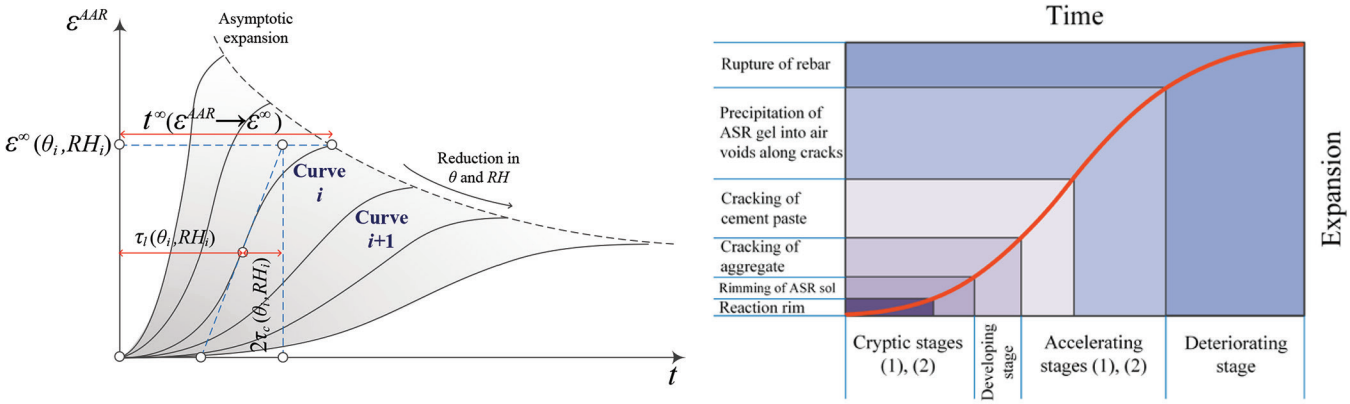

(a) Effect of temperature and relative humidity,

(b) Physical interpretation

Fig. 2—AAR expansion curve.[30]

where τ_l and τ_c are the latency and characteristic times, respectively. The former corresponds to the inflexion point and the latter is defined in terms of the intersection of the tangent at τ_l with the asymptotic unit value of ξ (Fig. 2(a)). They are given by

$$\tau_l(\theta) = \tau_l(\theta_0)\exp\left[U_l\left(\frac{1}{\theta}-\frac{1}{\theta_0}\right)\right]$$
$$\tau_c(\theta) = \tau_c(\theta_0)\exp\left[U_c\left(\frac{1}{\theta}-\frac{1}{\theta_0}\right)\right] \quad (2)$$

expressed in terms of the absolute temperature (θ K = 273 + T°C) and the corresponding activation energies. U_l and U_c are the activation energies, minimum energy required to trigger the reaction for the latency, and characteristic times, respectively. Once the volumetric AAR strain is determined, it is decomposed into a tensorial strain in accordance to the three weight factors associated with the principal stresses. Finally, degradation of the tensile strength and elastic modulus is accounted for as follows

$$E(t,\theta) = E_0\left[1-\left(1-\beta_E\right)\xi(t,\theta)\right]$$
$$f_t'(t,\theta) = f_{t,0}'\left[1-\left(1-\beta_{f_t}\right)\xi(t,\theta)\right] \quad (3)$$

The model is relatively simple to implement in an existing finite element code and has been implemented in many others.[21-28]

In the context of this study, there are no good estimates for:

- What would be the ultimate AAR induced strain as possibly determined from reliable laboratory residual expansion test (not a simple task); and
- What is the internal relative humidity (RH) in the box girder.

Indeed, it has long been recognized that for AAR to occur, RH must be above a certain threshold.[29] The effect of temperature and relative humidity on the kinetics of the reaction is illustrated by Fig. 2(a), where the decrease in RH results in a decrease of peak AAR strain, while a decrease in temperature will slow the reaction. The engineering significance of the (sigmoid) expansion is illustrated in Fig. 2(b).[30]

FINITE ELEMENT MODEL

Based on the engineering report,[18] three zones were identified (Fig. 3). The top deck layer T is the warmest and has the maximum exposure to water, and hence is assigned the largest volumetric expansion ε^{∞}. The other two zones (C and B/S for center and bottom/side) are better protected from both the water and the radiant heat, and are thus arbitrarily (in the absence of a more rational criteria) assigned 80% and 70% of the deck value. Two quantum values were assigned

(as opposed to a continuously varying distribution to facilitate numerical simulation).

Thirteen reinforcement groups are identified (Fig. 4). Eight mm (0.31 in.) reinforcement for the lateral reinforcement (x-direction) spaced at 100 mm (3.94 in.) and at 125 mm (4.92 in.) from the external faces, and 7 mm (0.276 in.) at 125 mm (4.92 in.) for the rest. Also shown in the figure are the "index" points for which the finite element analyses will be recording the engineering demand parameters (EDPs) such as deformations and displacements.

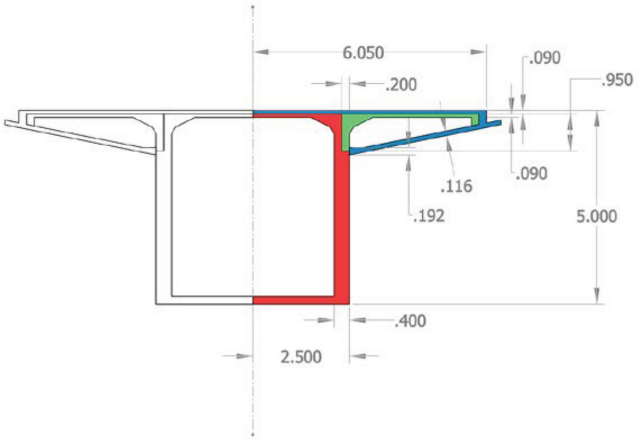

*Fig. 3—Modeled section identifying T, C, and B/S regions (blue, green, and red). (Note: For full-color version of figure, please refer to online PDF of paper at **www.concrete.org**.)*

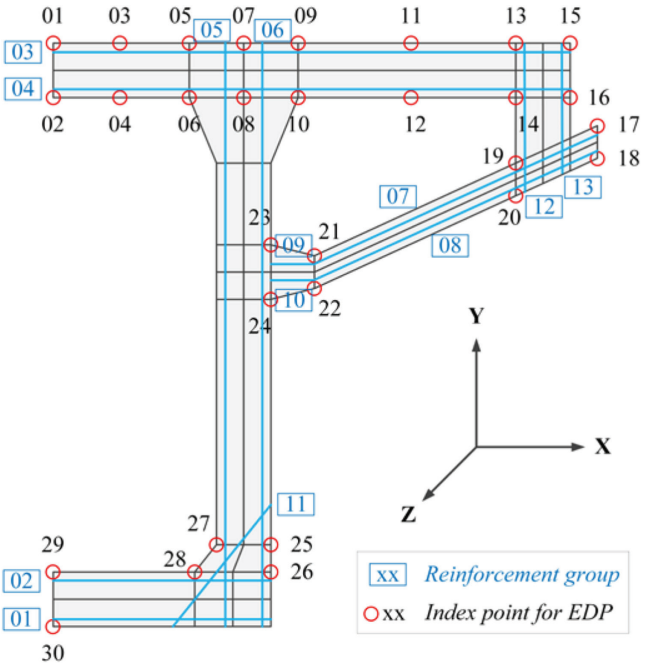

Fig. 4—Location of index points and reinforcing bar groups.

Because the computational cost for a probabilistic-based nonlinear finite element analysis of the viaduct will be prohibitive, and as this is the first attempt to provide such a solution, only one segment (half, by virtue of symmetry) of the bridge is modeled, and it is assumed to be fully supported at the base (Fig. 5).

The model has 6380 nodes and 4820 eight-node brick elements. There are 10 elements along the z-axis; four elements at the web (along the x-axis) and bottom (along the y-axis); and six elements at the top deck (along the y-axis). Overall, the mesh size is approximately 0.03 x 0.15 x 0.30 m (0.098 x 0.492 x 0.984 ft). Longitudinal displacements are constrained on the front and rear faces (z-axis), whereas free expansion is allowed along the lateral and vertical directions (x- and y-axis) except along the plane of symmetry (constrained in the x-direction) and along the base (in the y-direction), as the model assumed to be supported vertically. There are 10 layers in the longitudinal direction, and the mesh is sufficiently fine by at least four layers of elements to properly capture flexure in all segments. The self-weight is applied in the first increment, and it is rapidly overwhelmed by the response to concrete swelling due to the subsequent AAR increments.

Coupled with the previously described AAR model is a nonlinear damage-fracture constitutive model for the concrete[31] (smeared crack model) both implemented in the code Merlin.[32]

Given that the viaduct is 45 years old, the analyses seek to predict the incremental response over a total of 100 years. A time increment that is too short will be computationally prohibitive, and a time increment that is too long will result in gross imprecision. Hence, and following some parametric studies, a time increment (known as Analysis Time Unit [ATU] in the model) of 40.56 days was selected, resulting in 900 increments for each of the (implicit) analyses.

Selection of concrete physical properties is critical for this epistemic study, and they are tabulated in Table 2. The assignment of the AAR properties (Table 3) was more delicate and had to take into account the field measurements (Table 1). Again, different AAR volumetric expansions are assigned to the T, C, and B/S regions (Fig. 3) based on their relative

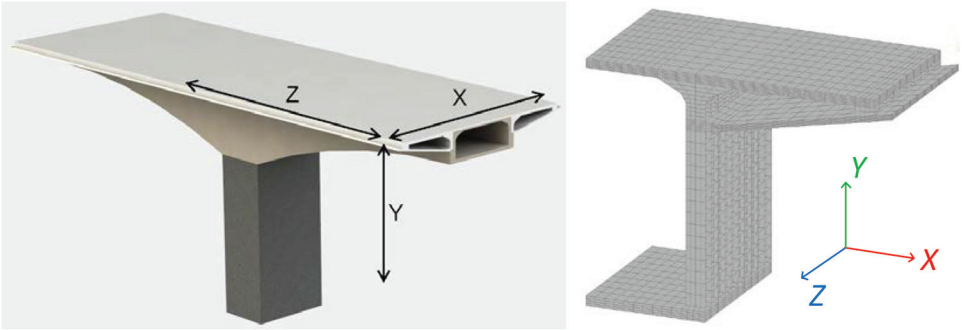

Fig. 5—Finite element mesh.

Table 2—Nonlinear concrete model[31] parameters

Characteristics	Symbol	Unit	Distributional model	Mean/COV	[min, max]
Mass density	ϱ	Gg/m^3	Deterministic	0.0024	—
Thermal expansion coefficient	α	1/°C	Deterministic	9.9×10^{-6}	—
Modulus of elasticity	E	MPa	Uniform distribution	40,000	[36,000, 44,000]
Poisson's ratio	ν	—	Deterministic	0.2	—
Tensile strength	f_t	MPa	Uniform distribution	4.5	[4.0, 5.0]
Exponential softening	G_F	MN/m	Normal distribution	1.2×10^{-4}/0.2	[9.0×10^{-5}1.5 × 10^{-4}]
Compressive strength (T and C)	f_c	MPa	Uniform distribution	–67.0	[–77.0, –57.0]
Compressive strength (B/S)	f_c	MPa	Uniform distribution	–78.0	[–88.0, –68.0]
Compressive critical displacement	w_d	m	Deterministic	–0.0005	—
Factor beta for return direction	β	—	Deterministic	0	—
Factor e for roundness of failure surface	e	—	Normal distribution	0.60/0.15	[0.5, 1.0]
Onset of nonlinearity in compression	f_{c0}	MPa	Normal distribution	–20/0.1	[–24, –16]
Plastic strain at compressive strength	ε_{cp}	—	Deterministic	–0.001	—

Notes: 1 Gg/m^3 = 62450 lb/ft^3; 1 MPa = 145 psi; 1 N/m = 0.06852 lbf/ft; (9/5)°C + 32 = °F; 1 m = 3.28 ft = 39.37 in.

Table 3—Characteristics of AAR model

Characteristics	Symbol	Unit	Distributional model	Mean/COV	[min, max]
Maximum volumetric strain (T)	$(\varepsilon^{\infty}_{AAR})_T$	—	Trapezoidal	—	[0.004, 0.020]
Maximum volumetric strain (C)	$(\varepsilon^{\infty}_{AAR})_C$	—	Deterministic	80% × $(\varepsilon^{\infty}_{AAR})_T$	[0.0032, 0.016]
Maximum volumetric strain (B/S)	$(\varepsilon^{\infty}_{AAR})_{B/S}$	—	Deterministic	70% × $(\varepsilon^{\infty}_{AAR})_T$	[0.0028, 0.014]
Characteristic time	τ_c	ATU	Trapezoidal	—	[40, 75]
Latency time	τ_l	ATU	Trapezoidal	—	[480, 610]
Activation energy associated with τ_c	U_C	K	Uniform distribution	5400	[4900, 5900]
Activation energy associated with τ_l	U_L	K	Uniform distribution	9400	[8900, 9900]
Residual reduction factor	Γ_r	—	Normal distribution	0.15/0.2	[0.1, 0.2]
Fraction of ε_t prior to reduction of AAR expansion due to macro cracking	$_r$	—	Normal distribution	0.5/0.2	[0.3, 0.7]
Compressive strength (T/C)	f_c	MPa	Uniform distribution	–67.0	[–77.0, –57.0]
Compressive strength (B/S)	f_c	MPa	Uniform distribution	–78.0	[–88.0, –68.0]
Tensile strength	f_t	MPa	Uniform distribution	4.5	[4.0, 5.0]
Shape factor	a	—	Deterministic	–2	—
Reference temperature	T_0	°C	—	10.1	—
Upper compressive stress beyond which there is no more AAR expansion	σ_U	MPa	Deterministic	–8.0	—
Reduction fraction for Young's modulus (T/C)	β_E	—	Uniform distribution	—	[0.68, 0.78]
Reduction fraction for Young's modulus (B/S)	β_E	—	Uniform distribution	—	[0.45, 0.60]
Reduction faction for tensile strength (T/C)	β_{ft}	—	Uniform distribution	—	[0.18, 0.57]
Reduction faction for tensile strength (B/S)	β_{ft}	—	Uniform distribution	—	[0.10, 0.41]

Notes: 1 MPa = 145 psi; (9/5) K – 459.67 = °F; (9/5)°C + 32 = °F.

exposure to water. Selection of the controlling expansion (at the top) is discussed in the following. Likewise, different reduction (or degradation) factors are accordingly assigned based on findings summarized in Table 1.

The value of the average yearly temperature at the viaduct location is 11°C (52°F). Hence, laboratory values for τ_l and τ_c (measured at 38°C [100°F]) are adjusted per Eq. (2). As to the reinforcement, only the yield stress (in an elastic-perfectly plastic model) is considered variable and is assigned a normal distribution function with a mean of 248 MPa (36 ksi) and a range of [225, 250] MPa ([32.6, 36.3] ksi).

PRELIMINARY DETERMINISTIC ANALYSIS

A preliminary deterministic set of analyses were performed to assess the spatial distribution of the concrete properties and the corresponding computation time. As

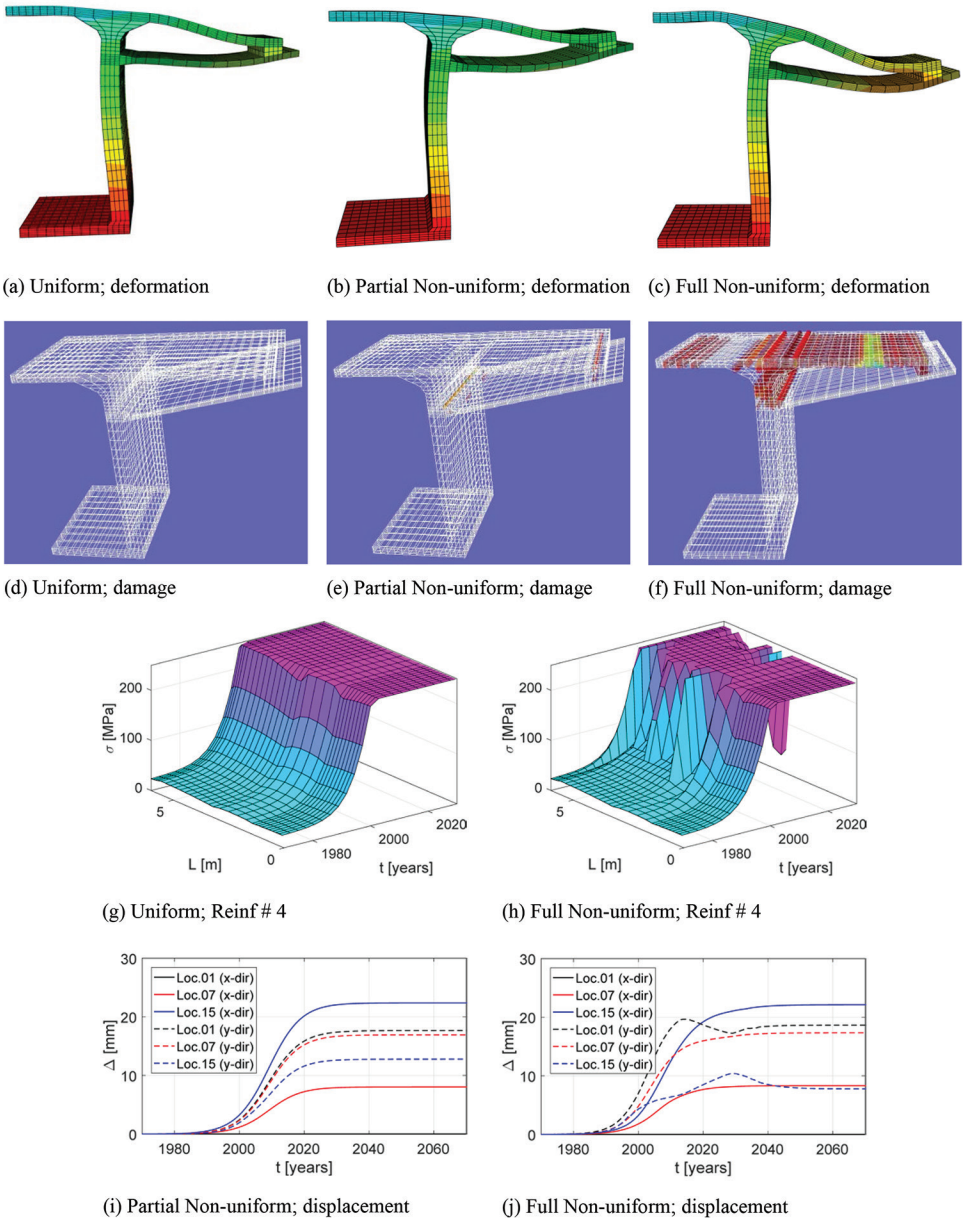

Fig. 6—Comparison of uniform, partial, and fully nonuniform models. (Note: 1 MPa = 145 psi; 1 m = 3.28 ft.)

stated earlier, three distinct zones of AAR exposure were identified (Fig. 3). Three sets of analyses were performed: 1) uniform (all concrete had the same ultimate expansion of 1%); and 2) and 3) second and third had 1.0%, 0.8%, and 0.7% expansion in each of the three regions (again, in light of varying exposure to water). While the second analysis had the same latency and characteristic times for all three regions, the third analysis had a varying set of latency and characteristic times.

Deformed shape, crack pattern, horizontal, and vertical displacements of three index points (1, 7, and 15 in Fig. 4) were scrutinized for all three analyses to better understand the impact of the nonuniform assignment of AAR properties (Fig. 6).

As expected, the more heterogeneous the concrete properties assigned, the more convoluted (and unpredictable) the deformed shape, from which one can identify zones of tensile and compressive stresses [Fig. 6(a), (b), and (c)], where the shaded surfaces correspond to the vertical displacement). In these analyses, the web undergoes relatively small flexure, and the inclined deck support appears to play an important role in the expansion. Induced (smeared) cracks at the end of the 900 increments (100 years, 1.0% volumetric strain) are shown in Fig. 6(d), (e), and (f). Consistent with the previous figures, the most realistic model (full nonuniformity) exhibits most cracks in the deck and the web-deck connection.

Figures 6(g) and (h) show the stress distribution along the center lateral top reinforcement (Group #4 shown in Fig. 4) in terms of time (as measured from the centerline) and location. As one would expect, the stress increases with time until it reaches the reinforcing bar yield stress. Of concern is that the yield stress is reached within the 45 years (that is, presently). This finding is caused by the high assumed final volumetric strain of 1.0%. The uniform case has only a small discontinuity, while the full nonuniform case exhibits strong stress jumps at the deck intersection with the supporting components. This finding was not anticipated and may be

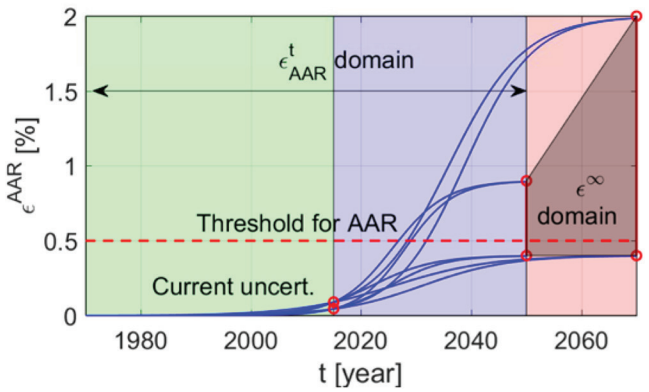

Fig. 7—Domain of investigation for AAR expansion (1970 to 2015: dry and 2016 to 2070: wet condition).

aggravated by the high value of assumed (in the absence of other indicators) expansion.

Finally, Fig. 6(i) and (j) show the lateral (x) and vertical (y) displacements of three index points—that is, Loc.01, Loc.07, and Loc.15 (Fig. 4). The displacement trend of the partial uniform case is very similar to the uniform one (not shown) but with smaller values. On the other hand, the displacement curves for the nonuniform case are slightly different. While the lateral displacement follows the same smooth sigmoid shape, the vertical displacements exhibit a peak, and then a "softening." *a priori* this could be attributed to a phase shift caused by the differences in the characteristic and latency times.

UNCERTAINTY QUANTIFICATION FRAMEWORK

To believe that one can perform a deterministic analysis of this bridge would be too presumptuous, as there are so many poorly quantified variables. Those are either aleatory in the nature of AAR, such as random distribution of pockets of high reactivity in the bridge, or they are epistemic because we do not fully know the concrete characteristic. In light of the aforementioned, a probabilistic investigation is undertaken. For the finite element investigation to be properly carried out, a mathematical representation of the kinetics should be given.

Consistent with the model presented earlier, the maximum volumetric strain ε^{∞} and the degradations of the elastic modulus and tensile strength β_E, and β_{ft} (Eq. (3)) must be determined in a manner consistent with the findings of the laboratory observations (Table 1).

Starting with ε^{∞}, and as previously mentioned, the estimated present expansion is less than 0.1%, and the future expansion at 90 years is expected to be in the range of 0.45 to 0.9%. Hence, for the sake of the analysis, it is assumed that the range of current expansion (after 45 years) is 10% of those values or 0.045 to 0.09%. As to the estimate of total expansion in the subsequent 35 (45 + 45 – 10) years (under most unfavorable conditions), it will be 0.45 to 0.9%. It should be noted that in laboratory tests, expansion follows a sigmoid curve (very low expansion initially, followed by a rapid increase), this may not be the case in the field. Furthermore, these guestimates originated from a petrographic examination of the concrete that may have indeed predicted was worst-case scenario. Finally, guesstimating for a total of 100 (45 + 45 + 10) years, the lower bound is maintained at 0.45% and the upper bound is 2.0% (again based on the reported 0.2 mm/m/y (2.4×10^{-3} in./ft/y) estimated from laboratory tests). Hence, the domain of uncertainties is illustrated by Fig. 7 broken in three zones: present, near, and far future.

Finally, having two points from current uncertainty and four points from the future one, eight potential expansion curves (marked as corner curves) are fitted, which are shown in Fig. 7.

At this point, a strategy must be devised on how to generate the random expansion curves for the Monte-Carlo simulation (MCS). The curves can be defined by three points: 1) the origin; 2) a random point at the current time (2015); and 3) a random point bound by the time interval of 2050 to 2070, and expansion intervals of 0.45 to 0.9% and 0.45 to 2.0%. The approach taken is heavily inspired by the LHS-wised technique of MCS.[33]

First, n_{sim} points are orderly identified within the (trapezoidal) domain of future uncertainly and another n_{sim} are randomly located within the axis of present uncertainty. Then, those points are randomly paired together, and along with the origin provide a set of three points that could uniquely define the expansion curve characterized by Eq. (1). The end point providing the time of reaction saturation and the maximum volumetric expansion ε^{∞}, a curve is then passed through those points (using a simple numerical algorithm) and τ_l, τ_c are determined (Fig. 8(a)).

Then, the corresponding distributions of the degradations must be defined as a set of random variables. Starting with f_t and E, the degradation model is given by Eq. (3) and must be calibrated with estimated material degradations shown in Table 1 defined as $M \pm m$. Hence, three sets of nonlinear least-squares optimizations are run to obtain the β values. Results are shown in Fig. 9.

Finally, a simple approach was adopted for the degradation of the compressive strength f_c, as the constitutive model does not currently account for its degradation. The average values of 67 and 78 MPa (9.7 and 11.3 ksi) (from Table 1, for top-center, and bottom/side, respectively) is taken as a mean with a range of ± 10 MPa (1.45 ksi).

So far, variables have been independently defined; however, there is a strong correlation among some of them. Unfortunately, there is no literature on what should be the correlation of key concrete parameters; hence, "engineering judgment" was exercised in assigning those correlation coefficients, ρ: $\rho(_{GF \leftrightarrow ft}) = 0.5$ $\rho(_{GF \leftrightarrow ft}) = 0.6$, $\rho(_{fc \leftrightarrow ft}) = 0.6$, $\rho(_{E \leftrightarrow fc}) = 0.6$, $\rho(_{Ul \leftrightarrow Uc}) = 0.6$, $\rho(_{\beta E \leftrightarrow \beta ft}) = 0.7$, and $\rho = 0.0$ for the rest. Please note that correlation coefficient varies between 0.0 (no correlation) and 1.0 (full correlation). The subscript presents that two RVs have a degree of correlation. In summary, this section has detailed how the material properties have been previously assigned in Table 2 and Table 3.

AUTOMATION OF PROBABILISTIC ANALYSIS

Automation of the procedure was performed through developed Matlab codes that read user-defined input files and generate output ones. For each output parameter, results

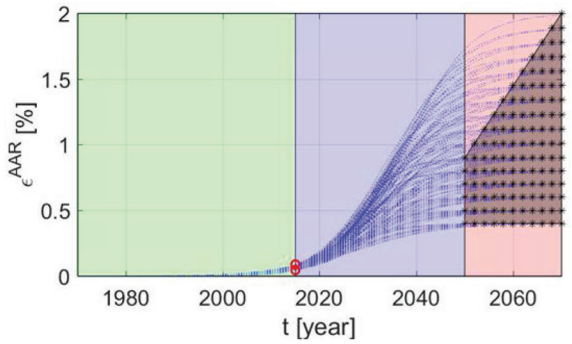

(a) LHS based sampling approach

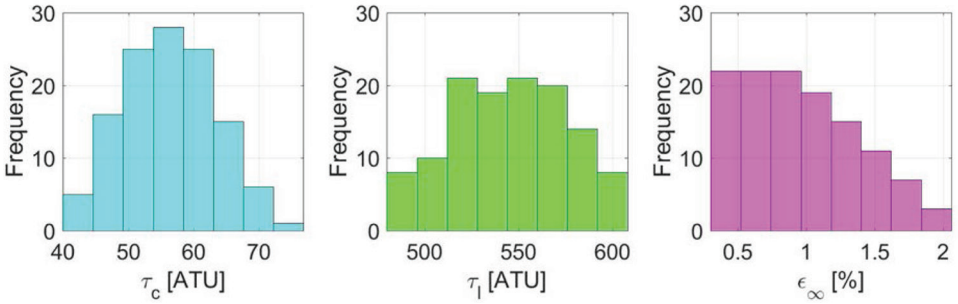

(b) Determined variable histograms

Fig. 8—Latin Hypercube-based sampling method.

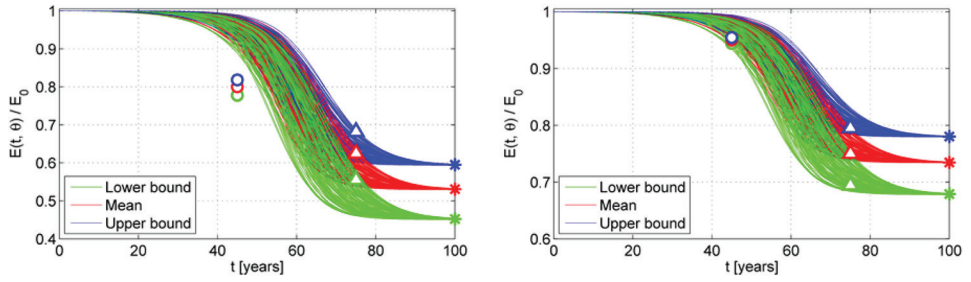

(a) β_E for bottom/side

(b) β_E for top/center

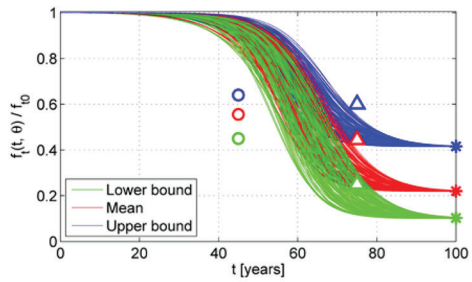

(c) β_{ft} for bottom/side

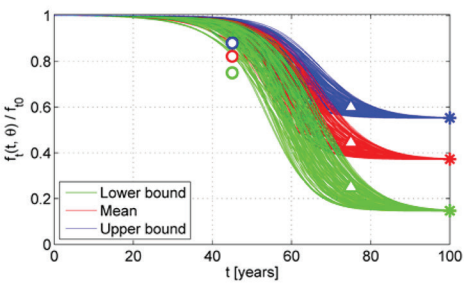

(d) β_{ft} for top/center

Fig. 9—Predicting degradation of E *and* f_t *based on optimization of experimental tests.*

are plotted along with their 16, 50, and 84 fractiles ranges (Fig. 10). This figure will provide the engineer with a rationale about the conditional behavior of the viaduct. The individual time-dependent simulations are shown with light gray lines, while the summarized curves are black. The vertical axis represents an EDP (for example, displacement, stress, and so on) and the horizontal axis is time (which is a metric for intensity).

ANALYSES RESULTS

An initial attempt to interpret results brought up an unanticipated set of two responses that resulted in two drastically different deformation shapes of this complex structure. Hence, the next section will examine the peculiar idiosyncrasy of the problem, and results of the 121 analyses will be addressed next.

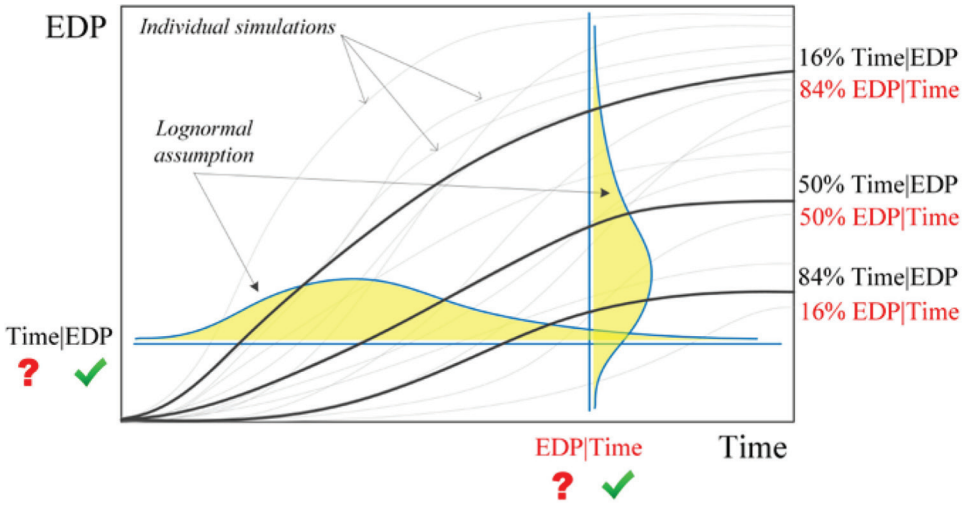

Fig. 10—Interpretation of results based on summarized curves.

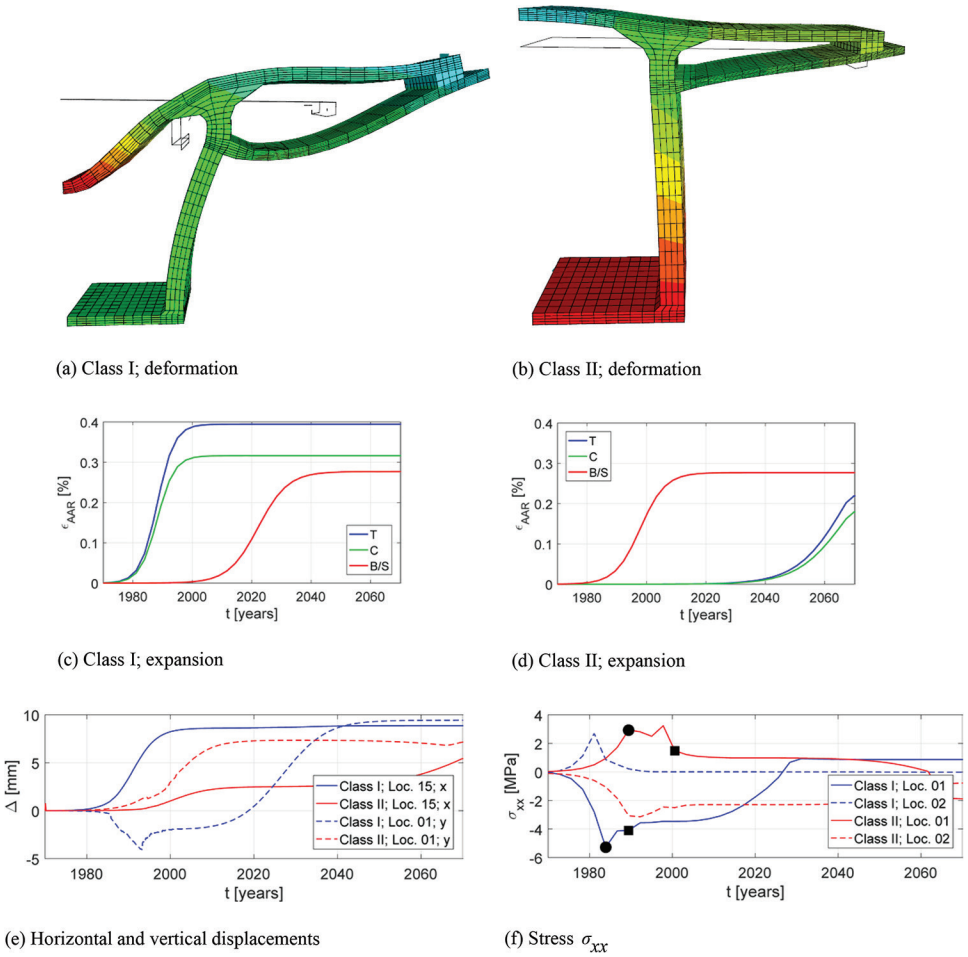

Fig. 11—Identification of two distinct structural responses attributed to delayed AAR expansion. (Note: 1 MPa = 145 psi; 1 m = 3.28 ft.)

Effect of kinetics

Scanning all 121 analyses results, two major deformation trends emerged, Fig. 11(a) and (b) (with colored shaded contour corresponding to the volumetric AAR expansion), tagged as Class I and II, respectively. In the first one, note the great "distortion" of the section with much flexure in both the flanges but also the web. In Class II, the vertical elongation of the web is clearly dominant, resulting in smaller curvatures in the web. Examining the corresponding (randomly generated in the context of the performed Monte-Carlo simulation with Latin Hypercube sampling) input data for each class of response, the cause was immediately attributed to the set of latency and characteristic times and the corresponding activation energies rather than with the values of ε^{∞} associated with different regions. From this set

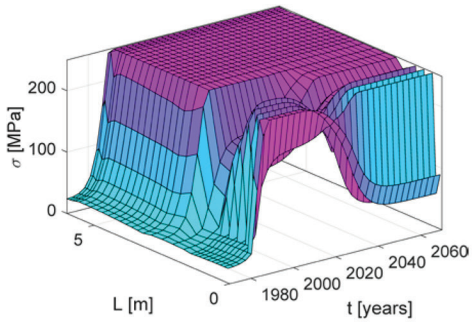

(a) Class I; rebar #4

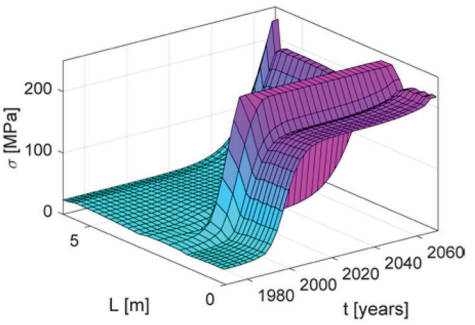

(b) Class II; rebar #4

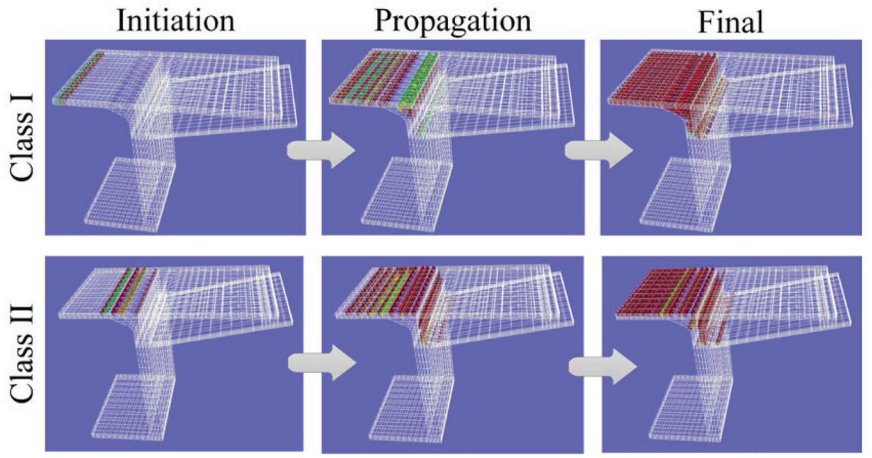

(c) Crack profile

Fig. 12—Reinforcing bar spatial and temporal stress distributions and cracking for two identified structural responses. (Note: 1 MPa = 145 psi; 1 m = 3.28 ft.)

of analyses, the importance of differential kinetics properties (used in Eq. (2)) was highlighted.

This cause was confirmed by Fig. 11(c) and (d), where the time lag in expansion among components is much more accentuated in the second, hence prioritizing the vertical expansion of the web in Class II. The displacements of the deck center line (Loc01) and edges (Loc15) in the y- and x-directions further illustrate this response (Fig. 11(e)). Time-wise, the vertical displacement of the deck center line in Class I moves downward for the first 25 years, and then with the stress release caused by cracking (Fig. 12(c)) it reverses and displaces upward.

The reinforcing bars (located at the bottom and across the deck) in Class I yield entirely after approximately 30 years (Fig. 12(a)). Again, locations are from the deck centerline. However, in Class II, reinforcing bars only partially yield in the vicinity of the center line. This is confirmed by the high curvature in the center part of the deck in Fig. 11(b). On the other hand, throughout most of the life span of the structure, the bottom reinforcement stress (away from the centerline) is very small for Class II (Fig. 12(b)). This finding is further supported by the absence of cracking in the corresponding part in Fig. 12(c), where in addition the crack initiation corresponds to discontinuity in stress diagram. In this figure, the crack initiation and propagation correspond to the solid circle and square points shown in stress time history curve (Fig. 11(f)).

PROBABILISTIC-BASED ASSESSMENT

The initial batch of 121 simulations yielded a set of 13 (approximately 10%) nonlinear analyses, which terminated prematurely due to lack of convergence. This was attributed to a randomly generated combination of (possibly) incompatible variables, which exhausted the capabilities of the models. Otherwise, CPU times ranged from 4 to 187 hours each, with a mean of 15.2 hours. Thus, the complete set of analyses required approximately 2 months of computations.

Following the earlier classification of analyses into two classes (I and II), 59 fell into the first and 49 into the second group. Out of the 30 index points with identifiable results (Fig. 4), only three EDPs are reported (Fig. 13(a)): the lateral (x) displacement at the edge of deck (Loc15), vertical displacement at the deck center line (Loc01), and the corresponding σ_{xx} stress. The maximum anticipated horizontal and vertical displacements are 43 and 30 mm (1.69 and 1.18 in.), and remain relatively small compared to the dimensions of the voussoir. The corresponding median 16th and 84th fractiles for each set of curves is also shown. Again, consistent with previous observations, the vertical displacements are higher for Class II, while they have lower lateral displacements. Finally, the stress reversal for Class II is worth noting. In all cases, the maximum tensile stress is capped by the ≅4 MPa (0.58 ksi) tensile strength specified. On the other hand, the compressive stresses are nearly negligible compared with the compressive strength of 67 MPa (9.7 ksi).

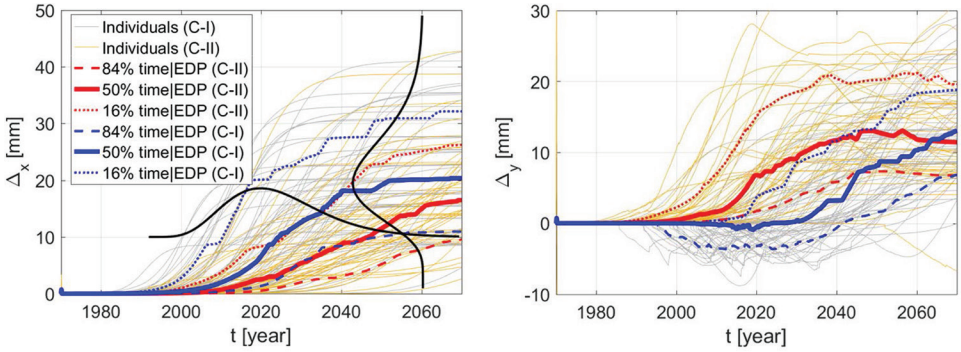

(a) Horizontal displacement; Loc15

(b) Vertical displacement; Loc01

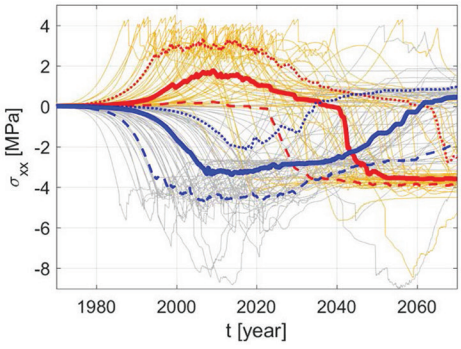

(c) σ_{xx} stresses; Loc01

Fig. 13—Individual probabilistic-based simulations and 16, 50, and 84% fractiles. (Note: 1 MPa = 145 psi; 1 m = 3.28 ft.)

Risk-informed condition assessment

This probabilistic-based analysis of a major infrastructure suffering from AAR can now serve as a vehicle to finally define the risk-informed condition assessment (RICA) of similar structure. Although this paradigm is not entirely new,[34] it has seldom been used in the context of evaluation of structures suffering from AAR. First, a few terms commonly used in earthquake engineering will be introduced.

Stressor, S—1) an incrementally increasing, cyclic, or time-dependent load (or displacement, acceleration, or pressure); or 2) an incrementally decreasing resistance parameter or degradation of strength properties. In earthquake engineering, S is typically called an intensity measure (IM) parameter. In the present paper, however, S is time. It is the increase in time that causes aging/deterioration of the concrete.

Response, R—As the name implies is merely the response of a structure to a stressor S. R may be either scalar or vectoral (single or multiple) damage variable (DV), such as drift or displacement. A limit state (LS) may be assigned to a DV and thus define a damage index (DI); for example, a stress (DV) should not exceed the strength (LS) according to a simple strength-based DI (otherwise, the result will be failure). In earthquake engineering, R is often referred as an EDP.

Capacity function—Relationship between S and R.

Fragility function—Continuous function showing the probability of exceedance of a certain LS for specific level of IM. This important concept was first introduced by Kennedy et al.[35] and is mathematically expressed as

$$\text{Fragility} = P\left[\text{LS} \mid \text{IM} = im\right] \tag{4}$$

where P $[A|B]$ is the conditional probability that A occurs given that B is equal to a particular im.

Figure 14(a) illustrates this concept typically used in earthquake engineering: What is the probability of a LS exceeding a certain value in terms of the seismic excitation, and what would be the corresponding level of damages? Similarly, for structures affected by AAR, Fig. 14(b) would be a corollary that gives the probability of a volumetric expansion exceeding a specified tensile strength with time.

Following these definitions, attention is returned to the problem previously analyzed. The DV is considered to be the vertical displacement (Fig. 13(a)) and an LS of 50 mm (1.97 in.) is assumed based on engineering judgment (that is, should the vertical displacement exceed 50 mm [1.97 in.], then the structure is considered to have locally failed). Then, as in Fig. 10, the temporal distribution of the DI is shown in Fig. 15(a), where six points are identified: the intersection of the 16th, median, and 84th fractiles with: a) a vertical line corresponding to the year 2040; and b) a horizontal one corresponding to a DI = 0.2 (or displacement of 10 mm [0.4 in.]). These values are arbitrarily selected for illustrative purposes. In actuality, they would be defined by the structure owner.

Two conditional assessments are then extracted: 1) time|DI; and 2) DI|time. The former is associated with the time needed for a given DI to occur (horizontal line), and the second the likelihood of a given DI occurring at a given time (vertical line) (Table 4).

From three fractiles, one can estimate the mean μ and the log-normal standard deviation β[36]

$$\mu_{\text{time}|\text{DI}} = \ln\left(\text{time}^{50\%}\right) \tag{5}$$

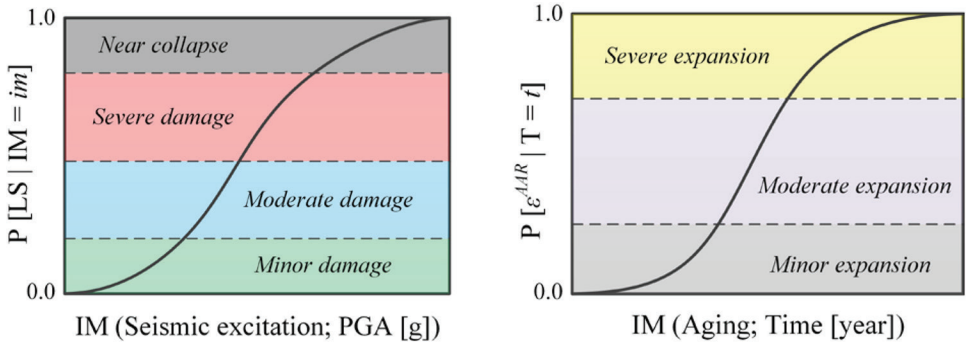

(a) Earthquake (b) AAR

Fig. 14—Fragility curves.

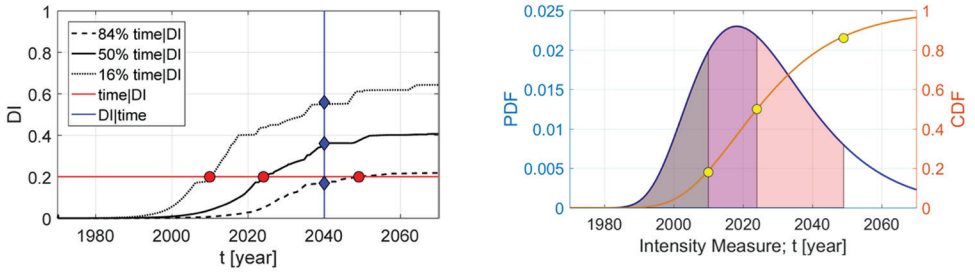

(a) 16, 50 and 86th Percentile temporal evolution of the DI (b) PDF and CDF for the DI

Fig. 15—Engineering interpretation of results.

Table 4—Central fractiles for two conditional assessments of Class I case; number inside parentheses represents absolute date

	Central fractiles		
Conditional assessment	16	50	84
time|DI [years]	40 (2010)	54 (2024)	79 (2049)
DI|time	0.17	0.36	0.56

$$\beta_{\text{time|DI}} \approx \frac{1}{2}\left(\ln\left(\text{time}^{84\%}\right) - \ln\left(\text{time}^{16\%}\right)\right) \quad (6)$$

which result in $\mu_{\text{time|DI}} = 3.99$ and $\beta_{\text{time|DI}} = 0.34$. From these values, the lognormal probability density function (PDF) and corresponding cumulative distribution function (CDF) are constructed (Fig. 15(b)). This last curve, for all practical purposes, is the fragility curve of the bridge assessed in terms of the DI of a potentially excessive displacement.

Similar curves could then be determined from other sets of quantities and engineers could meaningfully and rationally answer such basic and important questions as: a) how long would it take for a certain degradation to occur? or b) what is the degradation likely to occur at a given time? This is the essence of RICA presented in this paper for AAR.

CONCLUSIONS

Borrowing from the earthquake engineering literature, this paper presented a new paradigm to scientifically assess the integrity of structures affected by AAR. It is clearly a more palpable approach to regulators than the deterministic ones that are too often reported, and is relatively simple to perform. Indeed, this was made possible by the increased computational power available, and our ability to perform meaningful Monte Carlo simulation with sufficient reliability.

Another result that emerged from this investigation is the importance of properly modeling the kinetics of AAR in an incremental nonlinear analysis, and not limiting oneself to simply applying the maximum expansion. This analysis has highlighted the near impossibility to use intuition or "engineering judgment" to estimate the deformed shape (and thus location of stress concentration) given the idiosyncrasy of the complex model (nonuniform expansion, nonlinear time-dependent analysis, complex geometry). It should be pointed out that the main focus of this paper is not to make an accurate and reliable prediction of the future expansion (in light of the lack of reliable laboratory expansion measurements), but to use this bridge as a vector to introduce the paradigm of risk-informed assessment of structures affected by AAR.

AUTHOR BIOS

Mohammad Amin Hariri-Ardebili *is a Postdoctoral Research Associate and Adjunct Lecturer at the Department of Structural Engineering and Mechanics, University of Colorado Boulder, Boulder, CO. His research interests include performance-based earthquake engineering, probabilistic models, and life prediction of alkali-silica reaction.*

ACI member **Victor E. Saouma** *is a Professor of civil engineering at the University of Colorado. He is a member of ACI Committee 349, Concrete Nuclear Structures, and Joint ACI-ASCE Committees 446, Fracture Mechanics of Concrete, and 447, Finite Element Analysis of Reinforced Concrete Structures.*

Christine Merz *is a Petrographer and Geochemist with 25 years of experience in concrete technology, material testing, and structure assessment.*

ACKNOWLEDGMENTS

The second author would like to thank E. Brühwiler for hosting him during his sabbatical leave and for bringing to his attention the AAR issue in the analyzed viaduct, and for many preliminary discussions.

Thanks are also extended to the Swiss Federal Roads Office (FEDRO) for permission in using the field data, and finally to the US Nuclear Regulatory Commission for having made this study possible through an AAR-related grant (NRC-HQ-60-14-G-0010).

REFERENCES

1. West, G., *Alkali-Aggregate Reaction in Concrete Roads and Bridges*, Thomas Telford, London, UK, 1996.

2. Plum, N. M., "Tentative Recommendations for the Prevention of Alkali Aggregate Reactions," Danish Building Research Institute, 1961.

3. Miyagawa, T.; Seto, K.; Sasaki, K.; Mikata, Y.; Kuzume, K.; and Minami, T., "Fracture of Reinforcing Steels in Concrete Structures Damaged by Alkali-Silica Reaction—Field Survey, Mechanism and Maintenance," *Journal of Advanced Concrete Technology*, V. 4, No. 3, 2006, pp. 339-355. doi: 10.3151/jact.4.339

4. Montez, C., and Stokes III, W. E., "6th Street Viaduct Seismic Improvement Project; Environmental Impact Report," *Technical Report* INL/EXT-15-36425, City of Los Angeles and State of California Department of Transportation, Idaho Falls, ID, 2009.

5. Barbosa, R. A.; Hansen, S. G.; Hansen, K. K.; Hoang, L. C.; Grelk, B.; and Maag, I., "Assessment of Severely ASR Damaged Bridges: From Diagnosis to Structural Effects," *Proceedings of the 15th International Conference on Alkali-aggregate Reaction in Concrete (15th ICAAR)*, 2016.

6. Schmidt, J. W.; Hansen, S. G.; Barbosa, R. A.; and Henriksen, A., "Novel Shear Capacity Testing of ASR Damaged Full Scale Concrete Bridge," *Engineering Structures*, V. 79, 2014, pp. 365-374. doi: 10.1016/j.engstruct.2014.08.027

7. Shayan, A.; Xu, A.; and Andrew, P. H., "Implications of Alkali-Aggregate Reaction for Three Concrete Bridges," Concrete Institute of Australia Conference, Melbourne, Victoria, Australia, 2015.

8. Rivard, P., and Ballivy, F., "Quantitative Assessment of Concrete Damage due to Alkali-Silica Reactions (ASR) by Petrographic Analysis," 11th International Conference on Alkali Aggregate Reaction, 2000, pp. 889-898.

9. Lukschova, S.; Prikryl, R.; and Pertold, Z., "Petrographic Identification of Alkali-Silica Reactive Aggregates in Concrete from 20th Century Bridges," *Construction and Building Materials*, V. 23, No. 2, 2009, pp. 734-741. doi: 10.1016/j.conbuildmat.2008.02.020

10. Merz, C., and Leemann, A., "Assessment of the Residual Expansion Potential of Concrete from Structures Damaged by AAR," *Cement and Concrete Research*, V. 52, 2013, pp. 182-189. doi: 10.1016/j.cemconres.2013.07.001

11. FHWA, "Report on the Diagnostis, Prognosis, and Mitigation of Alkali-Silica Reaction (ASR) in Transportation Structures," *Technical Report FHWA-HIF-09-004*, Federal Highway Administration, Washington, DC, 2010.

12. Omikrine, M.; Kchakech, B.; Lavaud, S.; and Godart, B., "A New Model for the Analysis of the Structural/Mechanical Performance of Concrete Structures Affected by DEF—Case Study of an Existing Viaduct," *Structural Concrete*, V. 17, No. 6, 2016, pp. 1104-1113. doi: 10.1002/suco.201500181

13. Huang, Q.; Gardoni, P.; Trejo, D.; and Pagnotta, A., "Probabilistic Model for Steel-Concrete Bond Behavior in Bridge Columns Affected by Alkali Silica Reactions," *Engineering Structures*, V. 71, 2014, pp. 1-11. doi: 10.1016/j.engstruct.2014.03.041

14. Wojslaw, K., and Wisniewski, M., "Nonlinear and Time Dependent Analysis of a Concrete Bridge Suffering from Alkali-Silica Reaction: A Case Study of the Elgeseter Bridge in Trondheim," MA thesis, Norwegian University of Science and Technology, Institutt for konstruksjonsteknikk, Trondheim, Norway, 2014.

15. Saouma, V.; Hariri-Ardebili, M.; Le Pape, Y.; and Balaji, R., "Effect of Alkali-Silica Reaction on the Shear Strength of Reinforced Concrete Structural Members—A Numerical and Statistical Study," *Nuclear Engineering and Design*, V. 310, 2016, pp. 295-310. doi: 10.1016/j.nucengdes.2016.10.012

16. Bruhwiler, E.; Bastien-Masse, M.; Muhlberg, H.; Houriet, B.; Fleury, B.; Cuennet, S.; Schar, P.; and Boudry, F., "Strengthening the Chillon Viaducts Deck Slabs with Reinforced UHPFRC," *IABSE Symposium Report*, V. 105, M. Maurer, ed., International Association for Bridge and Structural Engineering, 2015, pp. 1-8.

17. Bureau Technique PIGUET SA, "The Viaducts of Chillon (Switzerland)," *La Technique des Travaux*, 1971, pp. 47-60.

18. Kronenberg, P.; Hammerschlag, J.; Merz, C.; and Houriet, B., "A9 - Viaducs de Chillon; Diagnostic relatif a la reaction alcali-granulats du béton," Technical Report, TFB & Holcim & gvh, 2013.

19. Saouma, V., and Perotti, L., "Constitutive Model for Alkali Aggregate Reactions," *ACI Materials Journal*, V. 103, No. 3, May-June 2006, pp. 194-202.

20. Saouma, V., *Numerical Modeling of Alkali Aggregate Reaction*, CRC Press, Boca Raton, FL, 2013, 320 pp.

21. Pian, J.; Feng, Y.; Wang, J.; Sun, C.; Zhang, C.; and Owen, D., "Modeling of Alkali-Silica Reaction in Concrete: A Review," *Frontiers of Structural and Civil Engineering*, V. 6, 2012, pp. 1-18.

22. El Mohandes, F., and Vecchio, F., "VecTor3: A. User's Manual; B. Sample Coupled Thermal and Structural Analysis," Department of Civil Engineering, University of Toronto, Toronto, ON, Canada, 2013.

23. Rodriguez, J.; Lacoma Aller, L.; Martinez Cutillas, F.; and Marti Rodriguez, J., "Contribution to Theme A of the Benchmark Workshop: Effect of Concrete Swelling on the Equilibrium and Displacements of an Arch Dam," *Proceedings of the XI ICOLD Benchmark Workshop on Numerical Analysis of Dams*, Valencia, Spain, 2011.

24. Mirzabozorg, H., personal communication, 2013.

25. Pan, J.; Feng, Y.; Jin, F.; and Zhang, C., "Numerical Prediction of Swelling in Concrete Arch Dams Affected by Alkali Aggregate Reaction," *European Journal of Environmental and Civil Engineering*, V. 17, No. 4, 2013, pp. 231-247. doi: 10.1080/19648189.2013.771112

26. Huang, H., and Spencer, B., "Grizzly Model for Fully Coupled Heat Transfer, Moisture, Diffusion, Alkali-Silica Reaction and Fracturing Process in Concrete," 9th International Conference on Fracture Mechanics of Concrete and Concrete Structures; FraMCoS-9, V. Saouma, J. Bolander, and E. Landis, eds., Berkeley, CA, 2016.

27. Huang, H.; Spencer, B.; and Cai, G., "Grizzly Model of Multi-Species Reactive Diffusion, Moisture/Heat Transfer, and Alkali-Silica Reaction in Concrete," *Technical Report INL/EXT-15-36425*, Idaho National Laboratory, Idaho Falls, ID, 2015.

28. Ben-Ftima, M.; Sadouki, H.; and Bruhwiler, E., "Development of a Computational Multi-Physical Framework for the Use of Nonlinear Explicit Approach in the Assessment of Concrete Structures Affected by Alklai-Aggregate Reaction," 9th International Conference on Fracture Mechanics of Concrete and Concrete Structures; FraMCoS-9, V. Saouma, J. Bolander, and E. Landis, eds., Berkeley, CA, 2016.

29. Capra, B., and Bournazel, J., "Modeling of Induced Mechanical Effects of Alkali-Aggregate Reactions," *Cement and Concrete Research*, V. 28, No. 2, 1998, pp. 251-260. doi: 10.1016/S0008-8846(97)00261-5

30. Saouma, V.; Martin, R.; Hariri-Ardebili, M.; and Katayama, T., "A Mathematical Model for the Kinetics of the Alkali-Silica Chemical Reaction," *Cement and Concrete Research*, V. 68, 2015, pp. 184-195. doi: 10.1016/j.cemconres.2014.10.021

31. Cervenka, J., and Papanikolaou, V., "Three Dimensional Combined Fracture-Plastic Material Model for Concrete," *International Journal of Plasticity*, V. 24, No. 12, 2008, pp. 2192-2220. doi: 10.1016/j.ijplas.2008.01.004

32. Saouma, V.; Cervenka, J.; and Reich, R., Merlin Finite Element User's Manual, 2010, http://civil.colorado.edu/~saouma/pdf/users.pdf.

33. Iman, R., and Conover, W., "A Distribution-Free Approach to Inducing Rank Correlation among Input Variables," *Communications in Statistics. Simulation and Computation*, V. B11, No. 3, 1982, pp. 311-334. doi: 10.1080/03610918208812265

34. Ellingwood, B., "Risk-Informed Condition Assessment of Civil Infrastructure: State of Practice and Research Issues," *Structure and Infrastructure Engineering*, V. 1, No. 1, 2005, pp. 7-18. doi: 10.1080/15732470412331289341

35. Kennedy, R.; Cornell, C.; Campbell, R.; Kaplan, S.; and Perla, H., "Probabilistic Seismic Safety Study of an Existing Nuclear Power Plant," *Nuclear Engineering and Design*, V. 59, No. 2, 1980, pp. 315-338. doi: 10.1016/0029-5493(80)90203-4

36. Mood, A. M.; Graybill, F. A.; and Boes, D. C., *Introduction to the Theory of Statistics*, third edition, McGraw-Hill, New York, 1974.

37. Shayan, A., and Xu, A., "Comparison between In-Situ Expansion Measurements on AAR-Affected Beams, Drilled Cores and Large Sawn Sections," 14th International Conference on Alkali-Aggregate Reaction in Concrete (ICAAR), Austin, TX, May 2012.

ARE YOU A RESEARCHER?

SIGN UP FOR ORCID TODAY!

ORCID provides a persistent digital identifer that distinguishes you from every other researcher and, through integration in key research workflows such as manuscript and grant submission, supports automated linkages between you and your professional activities, ensuring that your work is recognized.

Individuals may use ORCID services freely and it's as easy as **1-2-3**:

1. REGISTER
2. ADD YOUR INFO
3. USE YOUR ORCID ID

For more information and to register, visit:

WWW.ORCID.ORG